UCLA
UCLA Electronic Theses and Dissertations

Title
A Three-dimensional Analysis to Investigate the Midface Changes with MSE

Permalink
https://escholarship.org/uc/item/4mh1s2h4

Author
Sfogliano, Luca

Publication Date
2019

Peer reviewed|Thesis/dissertation

eScholarship.org Powered by the California Digital Library
University of California

UNIVERSITY Of CALIFORNIA

Los Angeles

A Three-dimensional Analysis to Investigate the Midface Changes with MSE

A thesis submitted in partial satisfaction of the

requirements for the degree Master of Science

in Oral Biology

by

Luca Sfogliano

2019

© Copyright by

Luca Sfogliano

2019

ABSTRACT OF THE THESIS

A Three-dimensional Analysis to Investigate the Midface Changes with MSE

By

Luca Sfogliano

Master of Science in Oral Biology

University of California, Los Angeles, 2019

Professor Won Moon, Co-chair

and

Professor Sanjay M. Mallya, Co-chair

Maxillary width deficiencies are a common occurrence in orthodontic patients being one of the most pervasive skeletal problems in the craniofacial region. An early orthodontic treatment can improve a transverse as well as an anteroposterior maxillary discrepancy and it consists of a true skeletal expansion or of an arch development obtained through the orthodontic wire. A pure skeletal expansion can be achieved with conventional appliances when the palatal suture is not completely fused. The introduction of TAD's in common orthodontic practice has found several implications in the treatment of maxillary transverse deficiency. Using a micro-implants anchorage, the MSE has been proved to be a powerful tool to achieve a pure skeletal expansion even in adult subjects whose midpalatine maxillary suture is already fused.

Studies analyzing 2D measurements conducted on CBCT reported generalized changes in the skeletal structure of patients successfully treated with MSE, evidencing a more parallel expansion compared to the conventional expanders. These findings gave rise to the desire of closely studying the impact of MSE on the entire midface skeletal structure utilizing a pure three-dimensional approach.

Describing the three-dimensional movement that each bone undergoes during MSE is the major purpose of this study. No studies have previously used a pure tridimensional analysis to investigate the impact of MSE on the skeletal structures of the midface.

An innovative method for pure 3D analysis has been developed utilizing modern imaging software proving that Micro-Implant Assisted Maxillary Skeletal Expander (MSE) has a significant impact in the mid-facial bone structures.

The new analysis confirmed the previous finding obtained with 2D measurements and gave a better understanding of effect of MSE on the midfacial structures.

The thesis of Luca Sfogliano is approved.

Shen Hu

Carl A. Maida

Sanjay M. Mallya, Committee Co-Chair

Won Moon, Committee Co-Chair

University of California, Los Angeles

2019

TABLE OF CONTENT

LIST OF FIGURES

ACKNOWLEDGEMENTS

I would like to thank all the people who collaborated in this research, offering their support and contributing to my professional growth.

Particularly I want to thank Dr. Won Moon who gave me the opportunity to work in his lab at this exciting project. He stimulated my research with new inputs while continuously supporting me in my orthodontic residency and oral biology MS program. A special thanks goes to Dr. Ehab Bar for his constant help in the programing aspects of the research. This thesis could not have been completed without Dr. Moon and Dr. Bar innovative ideas and expertise. I would also like to thank Dr. Sanjay Mallya, Dr. Shen Hu and Dr. Carl Maida for agreeing to serve on my committee and Mr. Matthew Dingman for his administrative support.

Additionally, I want to acknowledge all the member of Dr. Moon lab and in particular Dr. Ney Paredes, Dr. Islam El-Kenawy, Dr. Andrew Fraser, Dr. Boshi Zhang and Dr. Tam Duong for their constant help and dedication with the past and ongoing researches.

Finally, a big thank goes to the dental students Joseph Bui, Rebecca Tsuei, Kody Kuo, Austin Williams, Eddie Bennett and Elianne Vazquez for their availability in helping with the tedious part of this project.

INTRODUCTION

Maxillary width deficiencies are a common occurrence in orthodontic patients, being in fact one of the most common skeletal problems in the craniofacial region[1,2,3]. A typical clinical finding in a patient with a constricted maxilla is a posterior crossbite[4]. This results in dark spaces at the corners of the mouth during smiling, commonly called buccal corridors. Another severe problem associated with a skeletally narrow upper arch is crowding, which can lead to an abnormal eruption pattern and consequently to teeth impaction. Relevant etiopathogenetic factors of the lack of transversal maxilla development are genetics, specifically through a polygenic multifactorial regulation and gene-environment interaction[5], and environmental influences as a result of abnormal function. The effects of breathing anomalies on maxillary growth are nowadays scientifically proven, reporting that patients with airway problems, like severe allergies or other respiratory issues, present with a narrow, V-shaped maxillary arch and a high palatal vault[6]. Digit habits that continue into the mixed dentition have also been linked to the development of posterior cross bite due to the increased amount of pressure from buccal musculature[7].

Traditionally, maxillary expansion can be divided into pure dental expansion, dental/skeletal expansion and a pure skeletal expansion. A satisfactory dental expansion can be achieved thanks to arch wire development or springs (quad-helix, bi-helix, Crozat). With screws like Hyrax, Haas or removable appliances, a combination of dental and skeletal expansion can be obtained[8,9]. Early orthodontic treatment can improve a transverse as well as an anteroposterior maxillary discrepancy and can consist of a true

skeletal expansion or arch development obtained through the orthodontic wire. Skeletal expansion can be achieved with the conventional appliance like Hyrax and Haas when the palatal suture is not completely fused affecting different sutures of the mid face[10,11,12,13]. Literature agrees that the successful rate of a maxillary skeletal expansion decreases getting further from the peak of growth but can be still achieved in young adults who still have a soft midpalatal suture[14].

However, both the Hyrax, as a tooth-anchored device, and the Haas, as a tooth- and tissue-anchored expander, inevitably produce buccal tipping of the teeth and bending of the bone on which they push on[15]. In adult patients with fused midpalatal sutures, the use of a traditional expander would result in dental tipping of the teeth used as anchorage. Thus, dental expansion in adults has anatomical limitations that can generate periodontal problems like dehiscence and fenestrations when expansion is not carefully planned and monitored. Relapse also represents a common concern when dental expansion is executed in adult patients.[16]

The only successful alternatives for a pure skeletal expansion are the conventional maxillary orthognathic surgery or the Surgical Assisted Rapid Palatal Expansion (SARPE), in which lateral maxillary wall corticotomy and midpalatal osteotomy are performed before activation of a conventional expander[17,18]. A satisfactory pure skeletal expansion can be achieved but costs and morbidity associated with a surgical procedure pose a significant concern. Moreover, the SARPE localizes its bony effects strictly to the lower maxilla, not reporting any important impact on the upper and middle 1/3rd of the midfacial region.

The introduction of Temporary Anchorage Devices (TADs) in common orthodontic practice has found several implications in the treatment of maxillary transverse deficiency[19]. Several orthodontists from all over the world have been in parallel developing Micro-implant assisted rapid palatal expanders (MARPE). Dr. Won Moon's Maxillary Skeletal Expander (MSE) belongs to this category and it is currently used as a valid alternative to SARPE in adult Patients[20,21] at the UCLA Orthodontics Clinic (Fig.1).

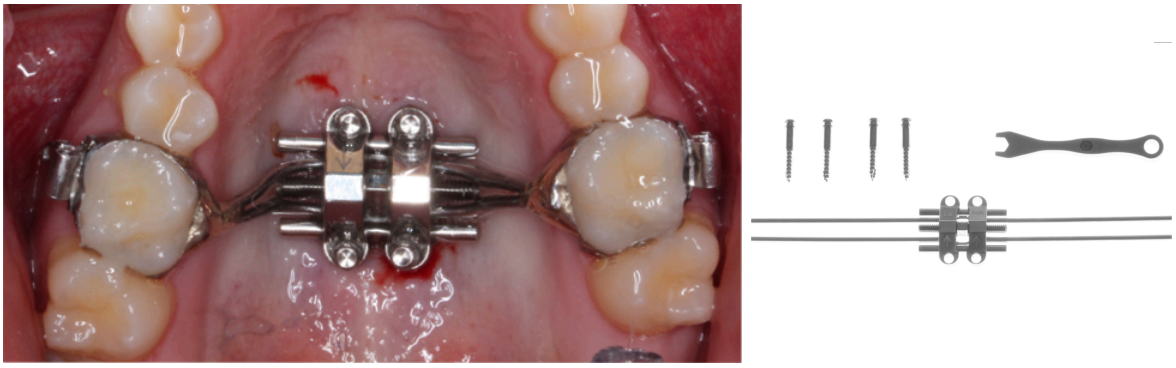

Fig. 1. MSE device (Biomaterials Korea Inc. Company). *Bands on the upper molars stabilize the appliance. The four TADs, placed perpendicular to the maxilla obtaining bi-cortical engagement, transmit the force to the entire maxillary complex. The two arms are made of soft metal to avoid dental tipping during the first phase of activation.*

The MSE appliance consists of two molar bands attached to the maxillary first molars and a central body containing an expansion jackscrew with 4 welded tubes (1.8mm diameter, 2mm length) attached. Four implants of 1.8mm in diameter and 11-13 mm in length are placed into the hard palate through the tubes. The key for a successful expansion, together with the mini-screw parallelism, is their bi-cortical engagement[22]: the proper length of the screw has to be selected carefully by analyzing the preliminary Cone Beam Computed Tomography (CBCT). The MSE skeletal anchorage following an ideal

TAD's placement leads to a parallel skeletal expansion with minimal dental tipping in patients whose midpalatal suture has already fused.

PRELIMINARY STUDIES

Many studies been conducted have been conducted on the MSE appliance and are currently proceeding in Dr. Won Moon's lab: case reports[20,21], impact of MSE on airway and inspiratory flow[23], 2D measurements on specific sutures[24,25,26] and molar tipping[27]. Some three-dimensional studies on the soft tissue changes related to MSE[28]and finite element models for skeletal effects with or without the use of protraction facemask have been produced[29,30].

Previous studies reported generalized changes in the skeletal structure of patients successfully treated with MSE, evidencing a more parallel expansion compared to the conventional expanders[22]. A coronal view of a two-dimensional superimposition on the cranial base, considered the most stable during growth and expansion,[31,32,33] shows the important changes that the midface undergoes after MSE (Fig.2).

Fig. 2. On-Demand 3D cranial base superimposition performed on the same Patient before and after MSE showing a generalized expansion of the entire maxillary complex. An asymmetrical expansion can be noticed.

These findings gave rise to the desire of closely studying the impact of MSE on the entire midfacial skeletal structure. A series of recent studies conducted by Dr. Won

Moon's Lab described the skeletal changes that the face undergoes with MSE using CBCT data and setting different planes as reference[24,25,26]. However, this study performed entirely two-dimensional measurements, not taking full advantage of the three-dimensional data obtained with CBCT (Fig. 3).

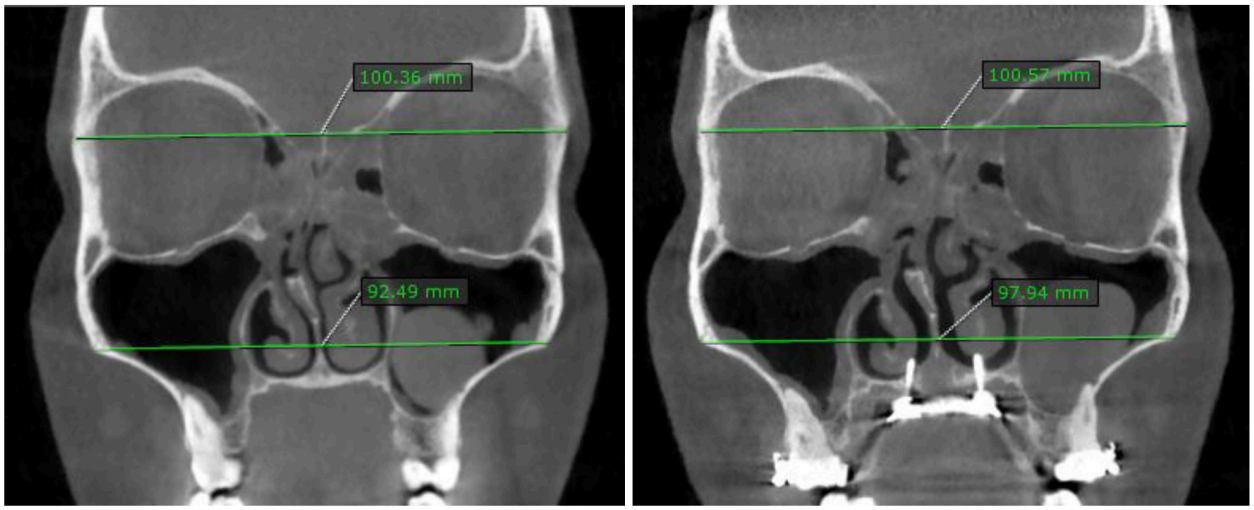

Fig. 3. Coronal zygomatic section (CZS) in a MSE patient. A: pre-expansion. B: post-expansion. Linear measurements: upper inter-zygomatic distance and lower inter-zygomatic distance. (Dr. D. Cantarella, Master of Science in Oral Biology Thesis - Skeletal effects induced by Maxillary Skeletal Expander (MSE) and Hyrax appliance in the midface[19]).

Converting a tridimensional image in two dimension and conducting measurements on each single CBCT slice will inevitably produce a loss of the data that is carried in the patient radiograph. The major purpose of this study is to describe three-dimensionally the movements that each bone undergoes during expansion. No studies have previously used a pure tridimensional analysis to investigate the impact of MSE on the skeletal structures of the midface.

However, 3D change quantification and averaging represent, to this date, one of the biggest challenges in 3D analysis. To be able to quantify these changes, surfaces of the skull pre- and post-expansion need to be extracted from the Digital Imaging and

communications in Medicine (DICOM) files and a 3D quantification has to be run on those files. One of the first steps to obtain accurate results between pre- and post-expansion data is performing an accurate registration among different timepoints (T0 and T1). Two major 3D registration methods are being currently used: volume/voxel-based and surface-based.

The voxel-based registration (VBR) is conducted directly on the DICOM file measuring the similarity of all geometrically corresponding voxel pairs. The surface-based registration (SBR) requires separate identification of corresponding surfaces in each of the images and is less straightforward than VBR[34].

Weissheimer et al.[35] tested the validity of the volume-based superimposition on OnDemand3D (Cybermed, Seoul, Korea) by measuring the differences when the same CBCTs were superimposed at the anterior cranial base and reported that the superimposition error was less than 0.5 mm. However, OnDemand3D (Cybermed, Seoul, Korea) does not perform segmentation after the registration and the registered DICOM files cannot be exported with the new orientation.

Ghoneima et al.[36] proved no statistical significance between volume-based and surface-based superimposition. Several segmentation programs are available (ITK-snap[37,38], 3D Slicer, Amira) and they all provide accurate and reliable surfaces (Fig.4) with some limitations attached to the quality of the DICOM that needs to be in balance with the patients' radiation exposure.

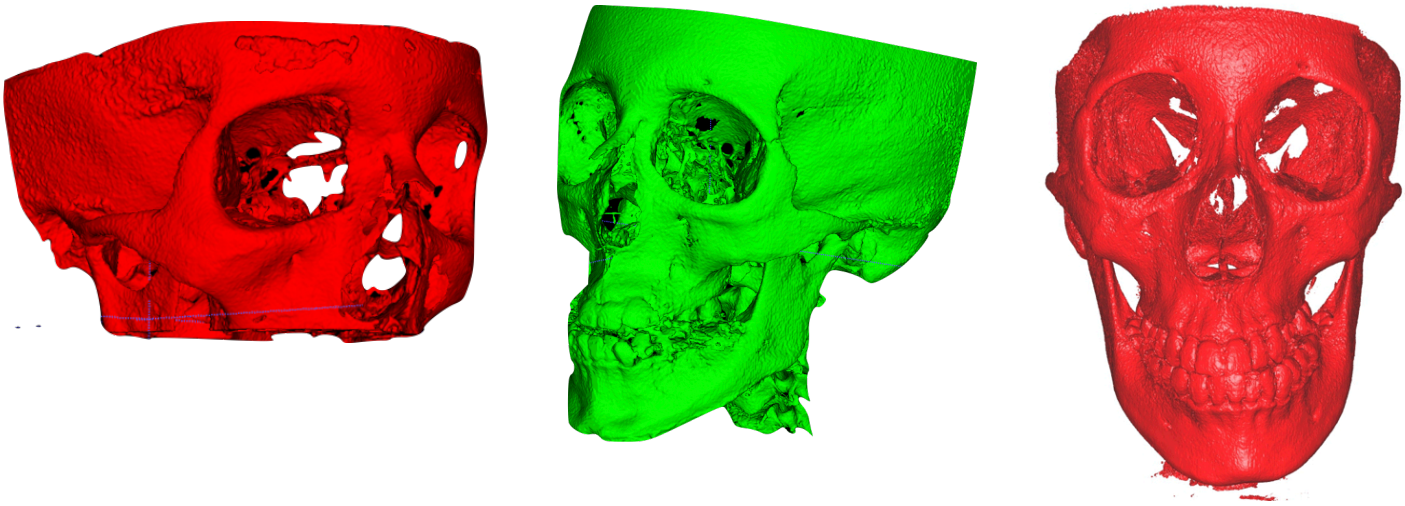

Fig. 4. Segmentation of .obj files obtained with ITK-snap, 3D slicer and Amira

3D surface mapping and quantification of the displacement between two different surfaces requires that the two objects are linked by a point-to-point correspondence. The same number of points have to be present on all the surfaces that need to be compared. The creation of a true point-to-point correspondence should be established but that represents one of the biggest challenges in morphometrics[39,40,41,42,43]. The closest point correspondence is easier to obtain but presents a lower degree of accuracy. When a surface moves from T0 to T1 not in a linear move, the closest point does not correspond to the true point and the most logical assumption is that the midfacial bone do not moves along a straight-line during expansion. A true point-to-point correspondence would increase the quality of the results (Fig 5).

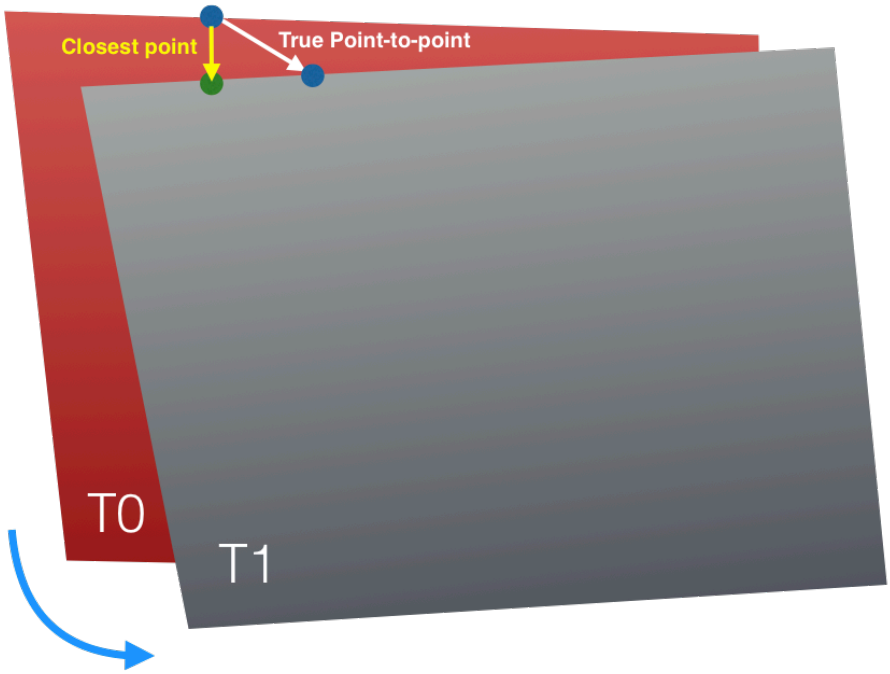

Fig 5. Difference between true point-to-point correspondence and closest point correspondence.

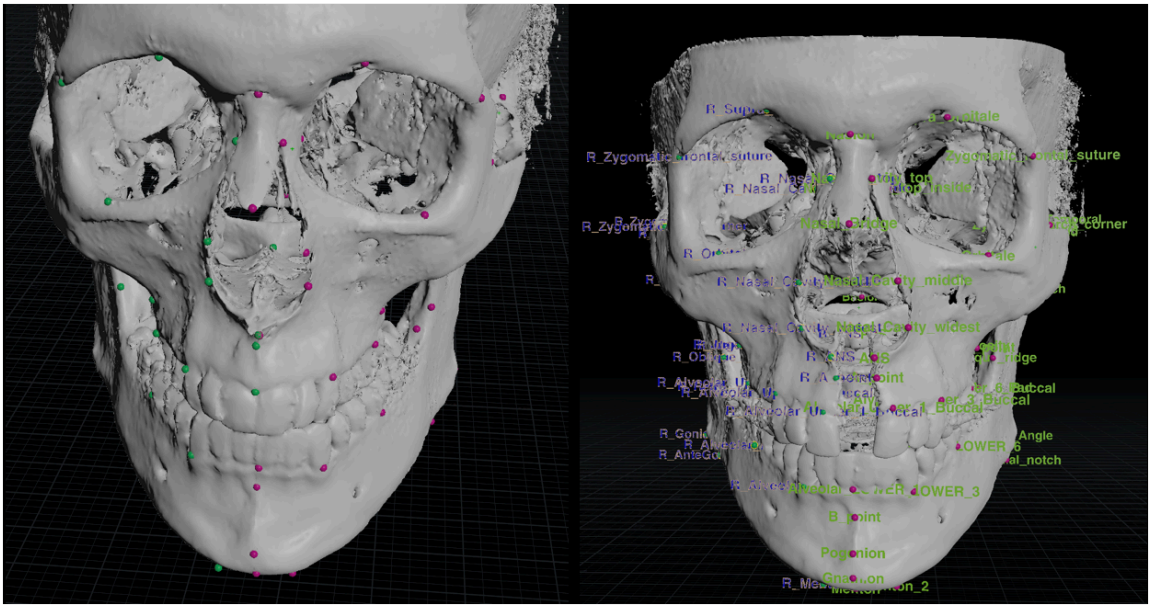

Fig. 6. Attempt of point plotting on pre- and post- segmented skulls to create a true point-to-point correspondence between the two skulls.

A way to obtain a more accurate point-to-point correspondence is to provide some reference and guidance to the software[44,45,46,47]. The use of manually positioned stable and well-defined landmarks added to the surfaces can be used to guide the creation of an accurate correspondence as showed in Figure 6.

OBJECTIVES AND SPECIFIC AIMS

The major purpose of this study is to provide a 3D model showing the skeletal midface changes related to Maxillary Skeletal Expander (MSE) treatment. This would lead to a complete understanding and prognosis of the movement that each bone undergoes during treatment with MSE: the development of an MSE expansion prediction-model that can be applied on clinical decision will be the final outcome of this research project.

The findings previously obtained via bi-dimensional analysis will be confirmed or confuted.

DESIGN AND METHODOLOGY

The aim of this project is to quantify the average change that happens to the skull and facial bone structure as a result of MSE. Such quantification is not a trivial task considering the complexity of the skull shape as well as the varying response to expansion that happens across different individuals. The process of quantification involves finding an average change in the skull shape in response to MSE. Computing this average change can be approached in two different ways:

1. Averaging all the pre-expansion samples to get an A(i) Skull. Averaging all the post-expansion sample an A(f) Skull. Compute the point to point correspondence between A(i) and A(f). Calculate the displacement vectors between A(i) and A(f). The problem with this method is the error in registration for all the pre-expansion samples. The post-expansion samples also exhibit the same error in registration because of the varied anatomical morphology between samples. Another error is introduced when registering the two averages together to calculate the average change.

2. The other method is to calculate the displacement vector between pre and post expansion for each individual sample (V). Register all the displacement vectors of all the samples together and get the point correspondence. Then average all the displacement vectors to calculate the average change. This method is more accurate than the earlier method because for each

individual sample, an accurate registration between the pre-expansion and post-expansion skull based on the cranial base.

Data collection

Pre- and post-CBCTs of 40 patients meeting the inclusion criteria (female or male, initial and post-expansion CBCTs available, successful expansion and no craniofacial anomalies) and treated with MSE at the Graduate Orthodontic Clinic of the UCLA School of Dentistry have been taken in the Oral Radiology department of the UCLA School of Dentistry. The CBCT scans were taken with a NewTom 5G (Verona, Italy) with an 18x16 field of view and 14-bit gray scale. Scan times were 18 seconds (3.6 seconds emission time), with 110 kV, utilizing an automatic exposure control that adjusts the milliampere according to the patient's bone density. Radiation exposure is controlled by the NewTom 5G Safebeam based on the patient's size. The CBCT data was rendered to produce .3mm slices.

IRB#17-000567 - *"Analysis of mini-implant assisted rapid palatal expansion (MARPE) or maxillary skeletal expansion (MSE) treatment pre- and post- expansion via cone beam computed tomography"* was used for this retrospective study.

The group of patients treated with MSE used for this study was composed of 40 subjects (14 males and 26 females) with a mean age of 18.2 +/- 4.2 years and an age range between 13.3 and 27.3 years.

Considering that the transverse dimension is already determined around 7 years of age for both males and females, growing patients have also been used. Moreover, post-expansion CBCTs were taken right after the completion of the required activation of the MSE appliance, when a satisfying transverse correction had been achieved. Consequently, the time frame between the two CBCT exams was insufficient for growth to have a significant impact on the midface.

Registration of DICOM data and segmentation into .obj with Amira

A voxel-based registration (VBR) has been performed using Amira 6.5.0 (Thermo Fisher Scientific, USA). After loading the DICOM data on Amira, the “Register Images” computation has been used to perform an automatic registration on the cranial base (Fig.7).

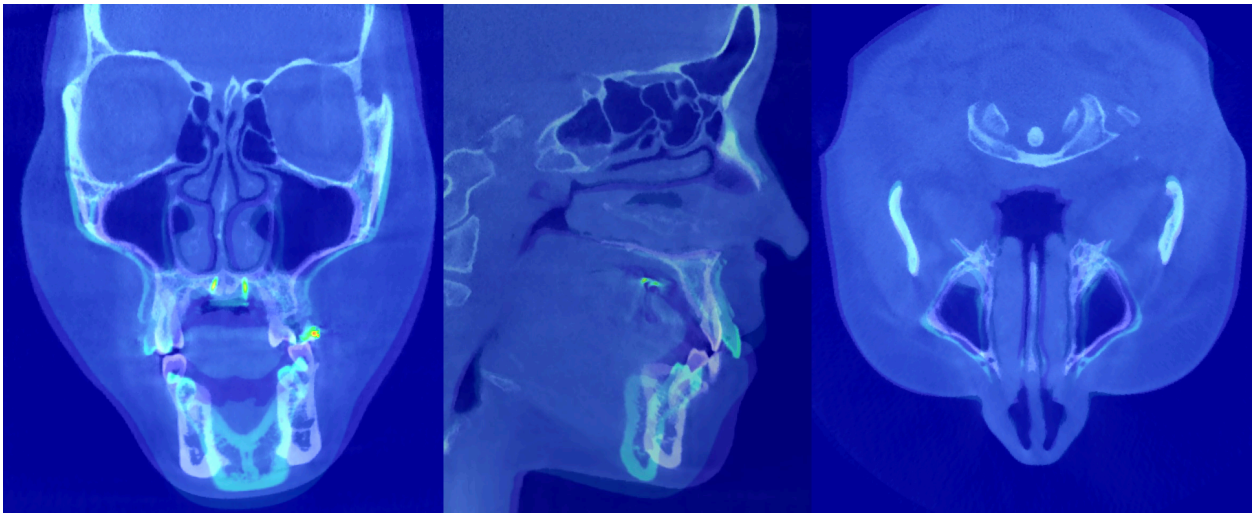

Fig. 7. Voxel-based registration (VBR) between pre- and post- DICOM file

After the registration, the DICOM have been segmented using the “Isosurface” command. Automatic segmentation has been obtained using a threshold between 450 and 700 according to the best quality segmentation. The same threshold has been maintained between T0 and T1 on the same subject (Fig.8).

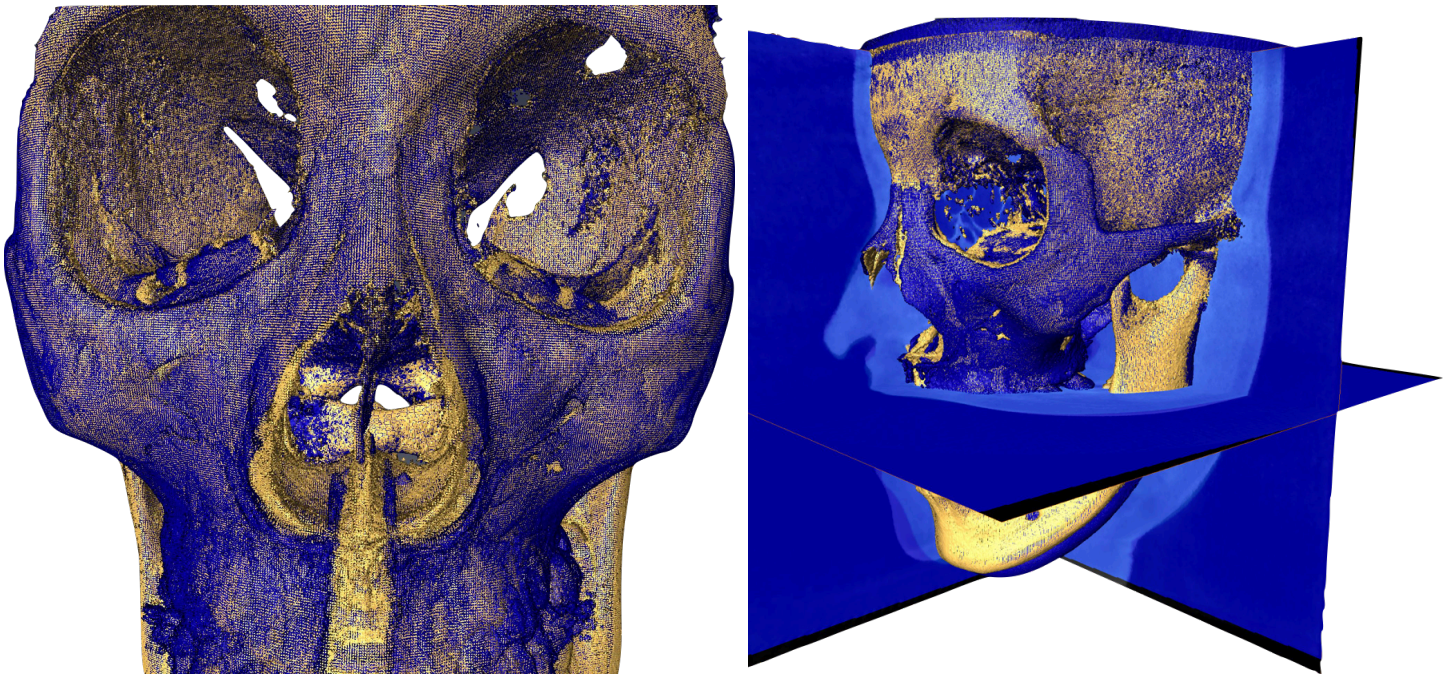

Fig. 8. Segmentation of T0 and T1 after registration

The generated surfaces have been exported as an “.obj” file while maintaining the same registration coordinate system. To be able to do so the “Resample Transformed Image” was used to reorient the T0-Dicom into the new coordinates (Fig. 9).

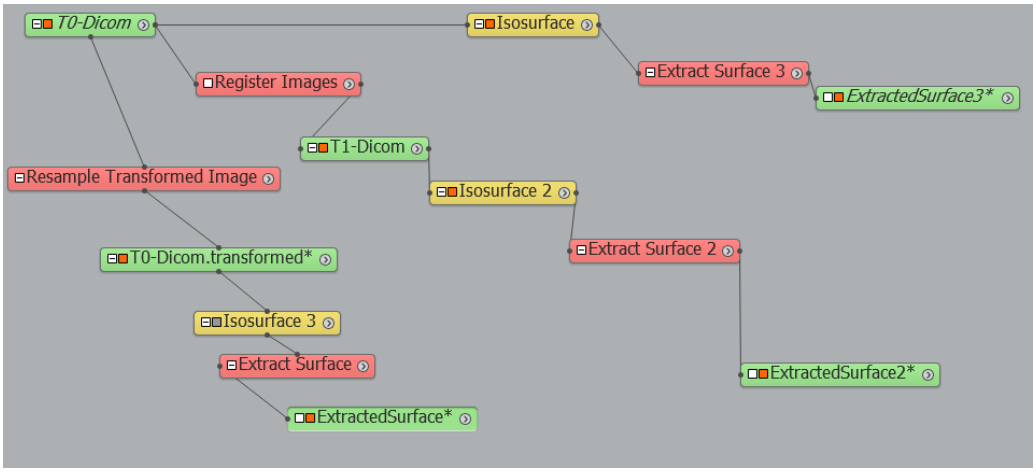

Fig. 9. Amira Pipeline used

HOUDINI

Houdini 17.5 (Side Effects Software Inc., Toronto, Canada), a 3D computer graphics software has been used to quantify and average the changes pre- and post- expansion.

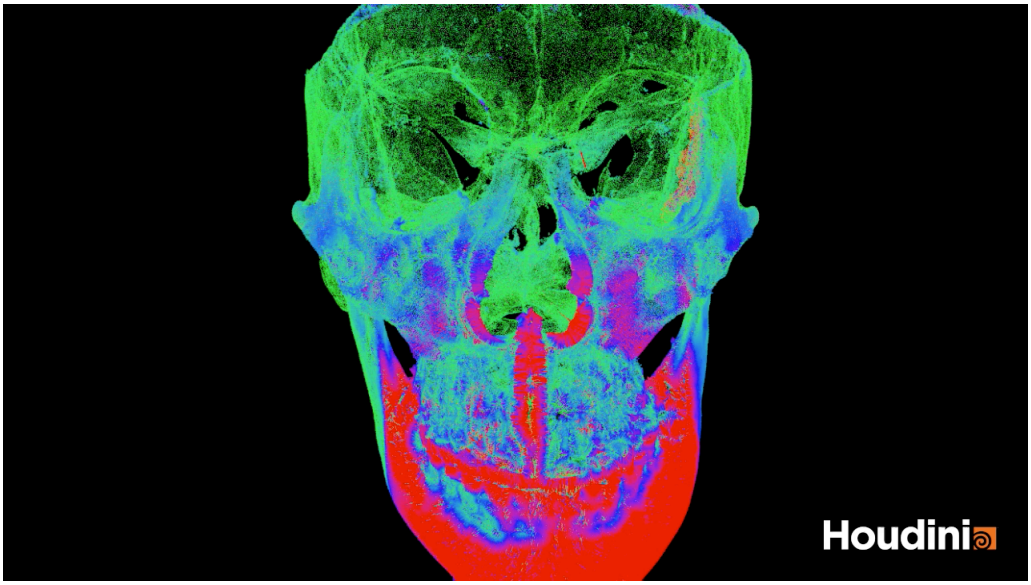

Fig.10. Vectors showing changes between Pre- (T0) and Post- (T1) expansion for one subject

Comparison and quantification

Comparison and quantification of the changes between pre-expansion and post-expansion surfaces for individual samples.

To create a point-to-point correspondence between pre-expansion and post-expansion skull, the following steps have been implemented in Houdini:

1. scatter one million points on each surface according to the surface area
2. For each point on the pre-expansion surface, the closest point on the post-expansion surface has been ray-traced
3. Compute the vector between the two corresponding points for each point on the surface.

The deformation or displacement vector *V is* defined as the vector between every point on the pre-expansion surface and its corresponding point on the post expansion surface. The vector *V* has three components (X,Y,Z) which are stored for each point.

The magnitude of the vector is stored in the *P-Value* parameter for each point that is a scalar value (i.e one variable) representing the amount of displacement that happened between a point on the pre-expansion surface and its corresponding point on the post-expansion surface (Fig. 11)

Compute the mean and standard deviation. The result is saved in the color value for each point where blue is 1 standard deviation and red is 2 standard deviations. There is a gradient from green to blue to red indicating values in between 0-1-2.

	P[x]	P[y]	P[z]	Cd[r]	Cd[g]	Cd[b]	N[x]	N[y]	N[z]	pscale	v[x]	v[y]	v[z]
0	95.6251	124.283	84.3599	0.0445819	0.630383	0.225035	0.0219163	0.419393	-0.183142	0.00919101	0.0219163	0.419393	-0.183142
1	95.6491	124.345	83.8404	0.0413258	0.607621	0.251053	-0.0037699	0.399219	-0.157659	0.0181681	-0.0037699	0.399219	-0.157659
2	95.8351	124.317	83.9598	0.0420678	0.613126	0.244806	0.00572733	0.426394	-0.154784	0.0199654	0.00572733	0.426394	-0.154784
3	95.9373	124.18	83.6807	0.0415457	0.608153	0.250301	0.0338024	0.380563	-0.164478	0.085645	0.0338024	0.380563	-0.164478
4	95.2943	124.557	84.0057	0.0433053	0.612879	0.243816	0.017703	0.381089	-0.168746	0.0532283	0.017703	0.381089	-0.168746
5	95.3744	124.47	85.1975	0.045342	0.612454	0.242204	0.0509614	0.465556	-0.186444	0.0144193	0.0509614	0.465556	-0.186444
6	95.8793	124.194	83.5243	0.0411103	0.608221	0.250668	0.0317278	0.376866	-0.169191	0.118128	0.0317278	0.376866	-0.169191
7	96.1848	124.361	84.0669	0.0421584	0.605769	0.252072	0.0201428	0.419922	-0.170422	0.0669698	0.0201428	0.419922	-0.170422
8	96.1633	124.104	83.4893	0.0425336	0.615758	0.241709	0.0154456	0.379397	-0.163076	0.00806496	0.0154456	0.379397	-0.163076
9	96.4236	124.168	83.7253	0.0425628	0.606109	0.251328	0.0524498	0.43227	-0.16258	0.074804	0.0524498	0.43227	-0.16258
10	95.9617	124.586	84.9402	0.0428561	0.614282	0.242862	0.0147433	0.429141	-0.147349	0.025125	0.0147433	0.429141	-0.147349
11	95.1504	124.763	84.8623	0.0466072	0.620154	0.233239	0.0497361	0.44654	-0.185607	0.0358932	0.0497361	0.44654	-0.185607
12	95.6232	124.295	83.6017	0.0416102	0.609028	0.249362	0.0237429	0.405482	-0.159043	0.023153	0.0237429	0.405482	-0.159043
13	96.481	124.079	83.5114	0.0427443	0.606448	0.250808	0.0327836	0.395016	-0.193129	0.0259756	0.0327836	0.395016	-0.193129
14	96.5861	124.214	84.016	0.0437739	0.612814	0.243412	0.0390013	0.447269	-0.175925	0.0349422	0.0390013	0.447269	-0.175925
15	96.3931	124.374	84.5775	0.0454749	0.623707	0.230818	0.0373669	0.38537	-0.165822	0.0223538	0.0373669	0.38537	-0.165822
16	95.7469	124.445	85.2776	0.043717	0.612223	0.24406	0.0277132	0.435172	-0.145285	0.0167457	0.0277132	0.435172	-0.145285
17	95.4153	124.734	85.6915	0.0488328	0.631369	0.219798	0.0190715	0.449923	-0.12362	0.0520081	0.0190715	0.449923	-0.12362
18	96.7473	124.094	83.7005	0.0430744	0.604798	0.252127	0.028104	0.494714	-0.199409	0.0427156	0.028104	0.494714	-0.199409
19	94.7896	124.899	84.374	0.0455924	0.600161	0.254246	0.0325832	0.429356	-0.201944	0.0118513	0.0325832	0.429356	-0.201944
20	95.3818	124.462	83.2055	0.0388305	0.599096	0.262073	0.000664563	0.397077	-0.146778	0.0393728	0.000664563	0.397077	-0.146778

Non-Commercial Edition

Fig.11. Information contained by each of the points on the surfaces

Saving the comparison file

The comparison file contains the following:

1. pre-expansion skull surface.
2. post-expansion skull surface.
3. Vector Displacement between pre and post surfaces:
    a. Direction of the vector (V)
    b. Magnitude of the vector (P-scale)
    c. Color (Cd) displacing standard deviation gradient

Registration of the comparison files

Registration of the comparison files together in the same coordinate space is an essential step before the averaging process.

Five points are plotted on the anterior cranial base (Fig. 12) of the comparison file of each sample:

- Anterior horns of sella turcica (2 points)
- Fronto-Zygomatico Sutures (Bilateral 2 points)
- Nasion (1 point)

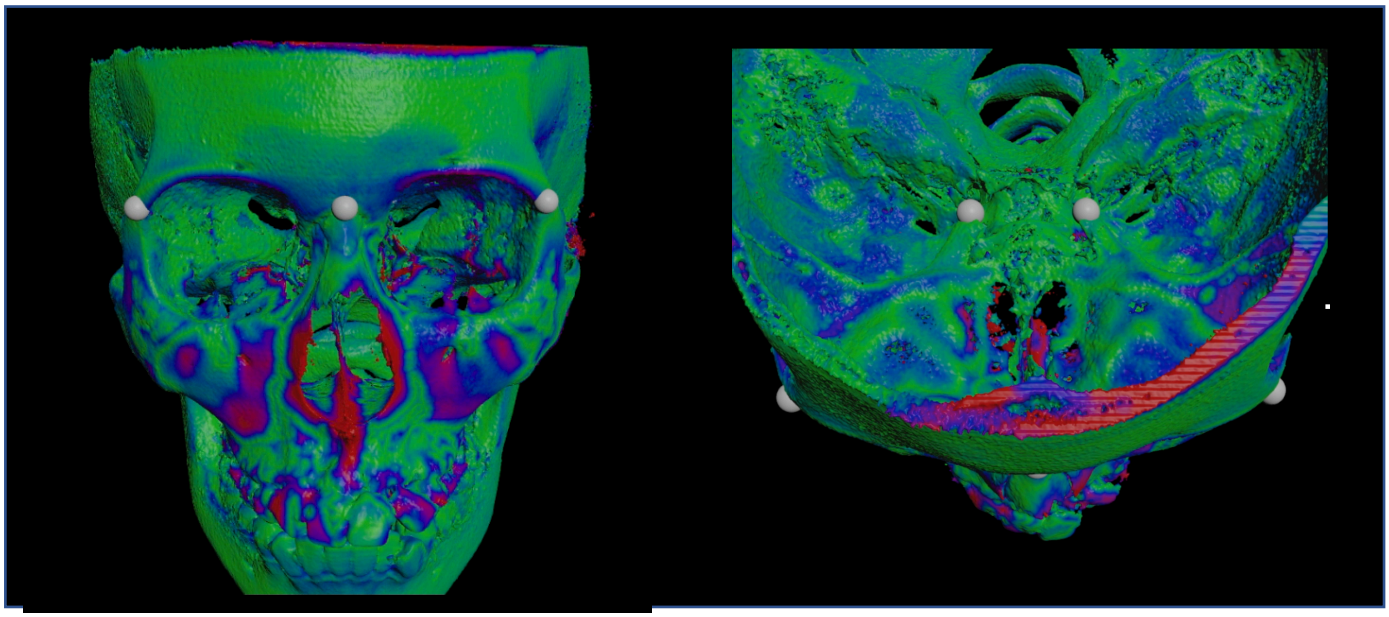

Fig.12. Points used to reorient samples into the 3D space

A Procrustes Superimposition of the samples based on the anterior cranial base registration is run and the comparison files are saved in the new coordinate system.

Atlas formation and point to point correspondence between samples

The point to point correspondence between different samples, or comparison files, needs to be established before an average is computed. The superimposed samples are loaded into Houdini and 1.000.000 points are scattered on each sample based on the surface area of the skull. The first sample is used as an atlas geometry that will serve as a template geometry against which all the other samples will be

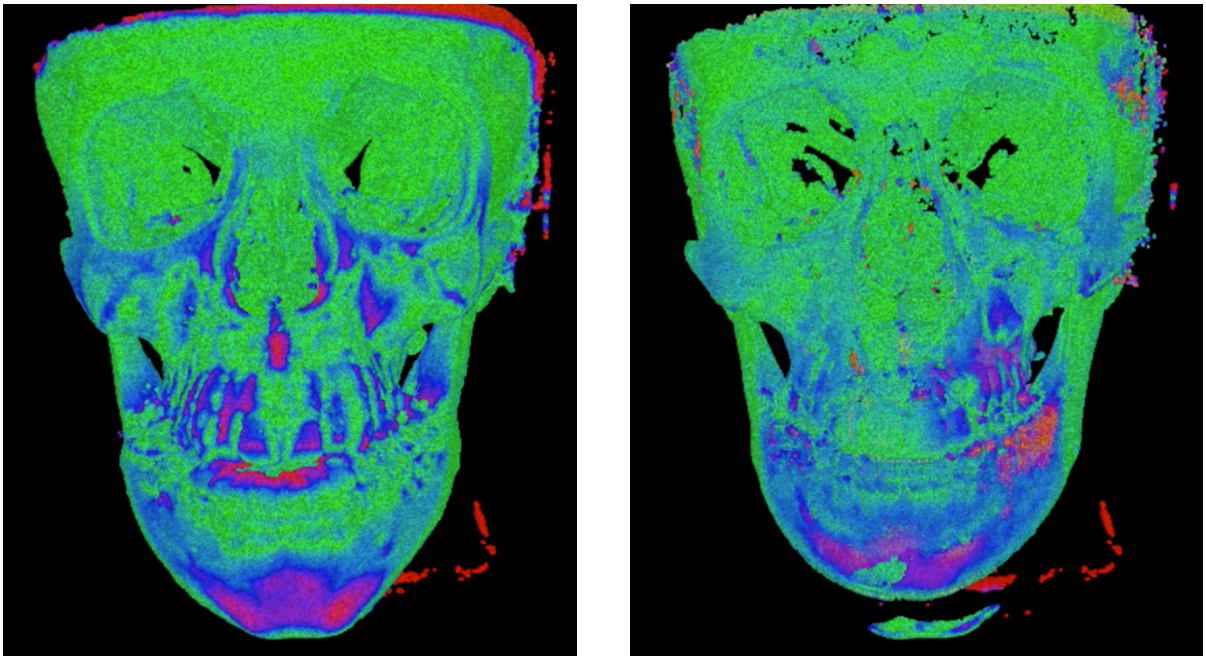

Fig.13. Atlas skull (Left) used to create correspondence with the other 39 samples

Mapped (Fig. 13). The basic concept of atlas mapping is to establish a point to point correspondence between the atlas geometry and all the other samples. The mapping process starts by running a tracing algorithm for each point on the atlas geometry where

the search area is a sphere with the radius 10 mm. The closet 50 points are chosen and an average is calculated for all the attributes associated with those 50 points and transferred to the point at the atlas geometry. The process is repeated for all the 1.000.000 points on the atlas surface.The atlas geometry is mapped on all the 40 samples and the result is saved to disk as (Atlas1-40).

Averaging the atlas-mapped samples

The average process of the samples is not as simple as averaging the (X,Y,Z) coordinated of the points on each sample. Each points has another set of information related to the earlier quantification between pre- and post expansion surfaces for each sample. All these embedded data has to be averaged together with the (X,Y,Z) coordinates of each point on the surface.

For each point on the surface, the following data is embedded in the geometry file:

1. Position [P]
2. Vector Displacement (V)
3. Pscale

Color (Green —> Blue —> Red) Blue = 1 std deviation, Red = 2 std deviations

All those attributes are averaged for each point on the surface.

RESULTS AND CONCLUSIONS

The current study presents an innovative method for 3D analysis and quantification. The measurements conducted via three-dimensional analysis show that palatal skeletal expansion with MSE is generated with a rotation of the entire maxillary complex around a fulcrum localized bilaterally in the frontozygomatic suture. These findings support our previous measurements and estimations obtained via bi-dimensional investigation.

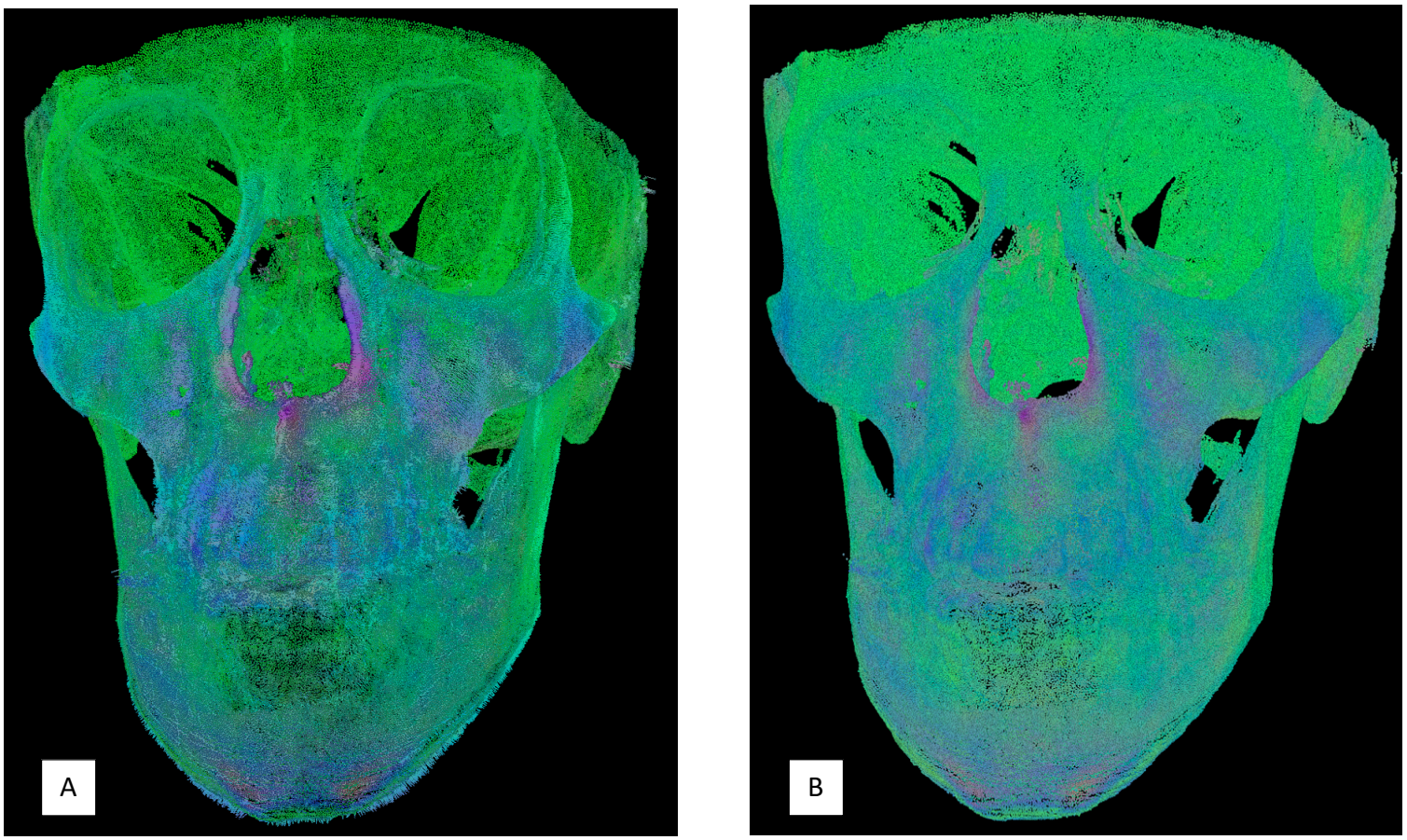

Fig. 14. Average changes between 40 patients displayed as vector map (A) and points (B); Green (0≤SD≤1), blue (1<SD≤2), red (SD>2)

The data can be visualized as vectors (Fig. 14 A), meshes or points (Fig. 14 B): the latter displaying not only the magnitude but also the direction of change.

The colorimetric gradients shown are in green for movements between 0 and 1 standard deviation ($0 \leq SD \leq 1$), blue between 1 and 2 ($1 < SD \leq 2$) and red above 2 ($SD > 2$). For instance, a bright green point signifies little to no movement (e.g. cranial base, posterior wall of the orbit, mastoid processes, etc.), whereas a red point indicates a larger movement (e.g. nasal cavity and mid-palatal suture).

Each of the 1 million vertices presents (Fig. 15):

- Position [P] of the initial skull in the 3 different coordinates (x, y, z)
- Color (Green, Blue, Red) expressed as a gradient with its different shades
- Vector Displacement V (=N. N is a value for visualization reasons only on Houdini, it helps in switching vectors to points). V and N display the direction of the movement that each point underwent during expansion in the three different axes (x, y, z). The coordinate of the post-MSE points can be detected through these values.
- P-scale (average of the change) = magnitude of the vector

	P[x]	P[y]	P[z]	Cd[r]	Cd[g]	Cd[b]	N[x]	N[y]	N[z]	pscale	v[x]	v[y]	v[z]
0	95.6251	124.283	84.3599	0.0445819	0.630383	0.225035	0.0219163	0.419393	-0.183142	0.00919101	0.0219163	0.419393	-0.183142
1	95.6491	124.345	83.8404	0.0413258	0.607621	0.251053	-0.0037699	0.399219	-0.157659	0.0181681	-0.0037699	0.399219	-0.157659
2	95.8351	124.317	83.9598	0.0420678	0.613126	0.244806	0.00572733	0.426394	-0.154784	0.0199654	0.00572733	0.426394	-0.154784
3	95.9373	124.18	83.6807	0.0415457	0.608153	0.250301	0.0338024	0.380563	-0.164478	0.085645	0.0338024	0.380563	-0.164478
4	95.2943	124.557	84.0057	0.0433053	0.612879	0.243816	0.017703	0.381089	-0.168746	0.0532283	0.017703	0.381089	-0.168746
5	95.3744	124.47	85.1975	0.045342	0.612454	0.242204	0.0509614	0.465556	-0.186444	0.0144193	0.0509614	0.465556	-0.186444
6	95.8793	124.194	83.5243	0.0411103	0.608221	0.250668	0.0317278	0.376866	-0.169191	0.118128	0.0317278	0.376866	-0.169191
7	96.1848	124.361	84.0669	0.0421584	0.605769	0.252072	0.0201428	0.419922	-0.170422	0.0669698	0.0201428	0.419922	-0.170422
8	96.1633	124.104	83.4893	0.0425336	0.615758	0.241709	0.0154456	0.379397	-0.163076	0.00806496	0.0154456	0.379397	-0.163076
9	96.4236	124.168	83.7253	0.0425628	0.606109	0.251328	0.0524498	0.43227	-0.16258	0.074804	0.0524498	0.43227	-0.16258
10	95.9617	124.586	84.9402	0.0428561	0.614282	0.242862	0.0147433	0.429141	-0.147349	0.025125	0.0147433	0.429141	-0.147349
11	95.1504	124.763	84.8623	0.0466072	0.620154	0.233239	0.0497361	0.44654	-0.185607	0.0358932	0.0497361	0.44654	-0.185607
12	95.6232	124.295	83.6017	0.0416102	0.609028	0.249362	0.0237429	0.405482	-0.159043	0.023153	0.0237429	0.405482	-0.159043
13	96.481	124.079	83.5114	0.0427443	0.606448	0.250808	0.0327836	0.395016	-0.193129	0.0259756	0.0327836	0.395016	-0.193129
14	96.5861	124.214	84.016	0.0437739	0.612814	0.243412	0.0390013	0.447269	-0.175925	0.0349422	0.0390013	0.447269	-0.175925
15	96.3931	124.374	84.5775	0.0454749	0.623707	0.230818	0.0373669	0.38537	-0.165822	0.0223538	0.0373669	0.38537	-0.165822
16	95.7469	124.445	85.2776	0.043717	0.612223	0.24406	0.0277132	0.435172	-0.145285	0.0167457	0.0277132	0.435172	-0.145285
17	95.4153	124.734	85.6915	0.0488328	0.631369	0.219798	0.0190715	0.449923	-0.12362	0.0520081	0.0190715	0.449923	-0.12362
18	96.7473	124.094	83.7005	0.0430744	0.604798	0.252127	0.028104	0.494714	-0.199409	0.0427156	0.028104	0.494714	-0.199409
19	94.7896	124.899	84.374	0.0455924	0.600161	0.254246	0.0325832	0.429356	-0.201944	0.0118513	0.0325832	0.429356	-0.201944
20	95.3818	124.462	83.2055	0.0388305	0.599096	0.262073	0.000664563	0.397077	-0.146778	0.0393728	0.000664563	0.397077	-0.146778

Non-Commercial Edition

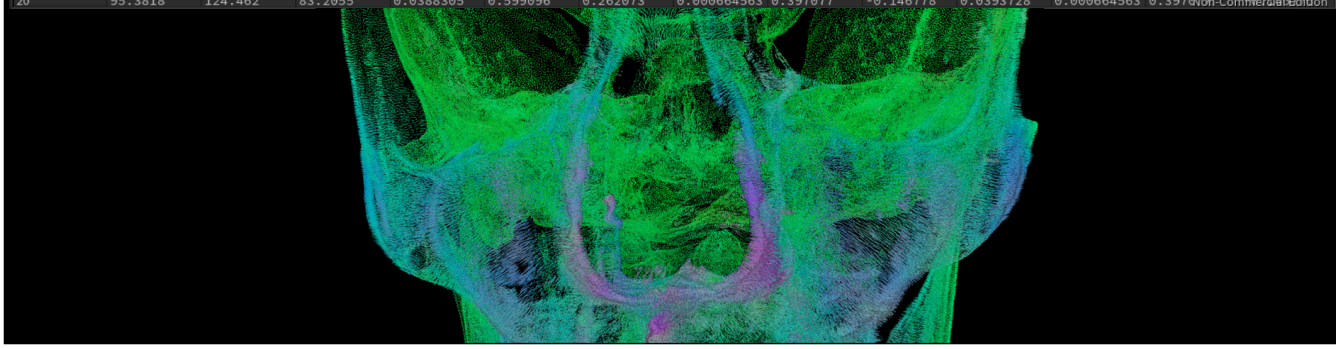

Fig. 15. Example of 3D data display for 21 points

To obtain a p-value map, each corresponding point in the different skulls will be incapsulated into a sphere that will represent the variance of that point equal to the dispersion of that point in the space in the separate samples. The smaller the radius of the sphere, the smaller the variance of that point. If a smaller variance is accompanied by high average change, high significance is showed (= high p-value) and vice versa: a bigger sphere and small average change show low significance and low p-value.

P-scale divided by variance for each point will give us the significance ratio. We map this ratio to percent and set our cutoff to the top 5% of significance (p-value >0.05). The remaining points have been hidden from the skull (Fig.16). Alternatively, a gradient or simplified colored p-value map could be created. A certain degree of asymmetry is noted with higher significance on the left midface in this group of patients.

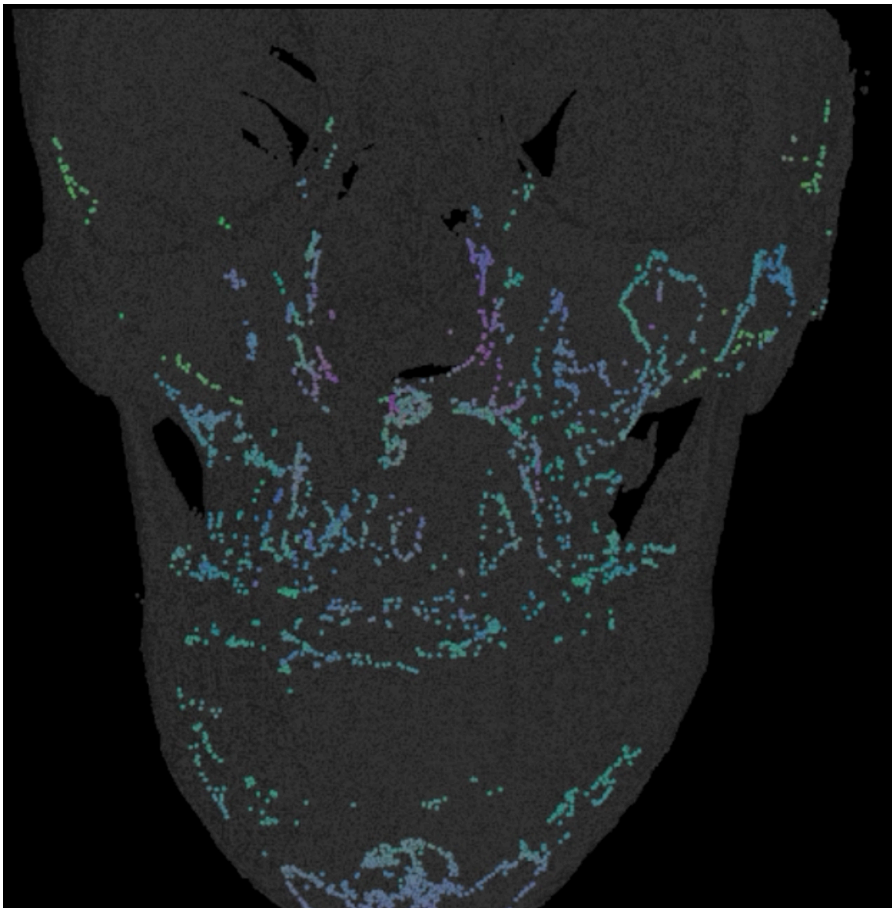

Fig.16. P-value map of 1,000,000 vertices presented on the skull surface with p-value >0.05

Micro-Implant Assisted Maxillary Skeletal Expander (MSE) demonstrates significant changes in the midfacial bone structures and the analysis conducted provides a much deeper understanding of the effects of MSE on the midface.

The Maxillary Skeletal Expander or MSE, designed by Prof. Won Moon, could rightfully be called Midfacial Skeletal Expander because of the generalized effect that it produces not only on the maxilla but also on the entire midface.

LIMITATIONS

This new methodology is highly promising but there are some limitations to consider. The quality of the CBCT is not accurate enough to capture high level details due the large field of view used in order to reduce patient exposure to radiation. Consequently, the segmented data present some noise related to the quality of the CBCT that could create some error in the quantification.

In addition, morphing all the skulls to an atlas and decreasing the number of vertices to 1,000,000 inevitably simplifies the surface, eliminating some of the data present in the segmented files and reducing the amount of information carried by the 3D files. However, 1 million points is a really high number compared to our initial expectations and a lot of data can still be extrapolated from them.

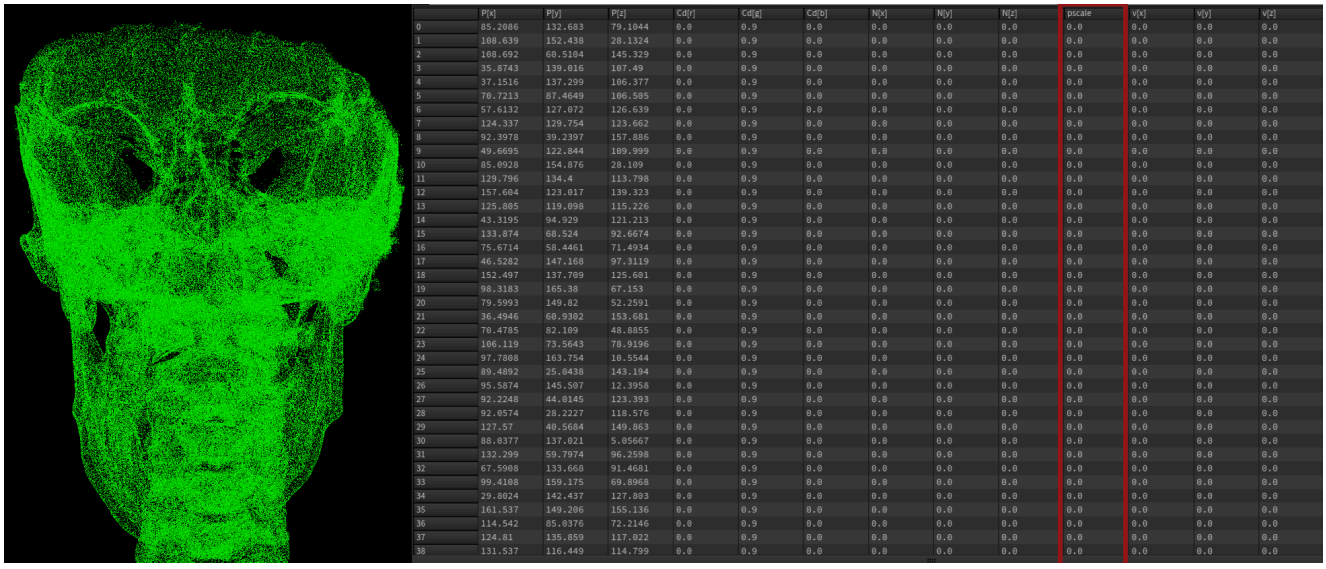

	P[x]	P[y]	P[z]	Cd[r]	Cd[g]	Cd[b]	N[x]	N[y]	N[z]	pscale	v[x]	v[y]	v[z]
0	85.2086	132.683	79.1044	0.0	0.9	0.0	0.0	0.0	0.0	0.0	0.0	0.0	0.0
1	108.639	152.438	28.1324	0.0	0.9	0.0	0.0	0.0	0.0	0.0	0.0	0.0	0.0
2	108.692	60.5104	145.329	0.0	0.9	0.0	0.0	0.0	0.0	0.0	0.0	0.0	0.0
3	35.8743	139.016	107.49	0.0	0.9	0.0	0.0	0.0	0.0	0.0	0.0	0.0	0.0
4	37.1516	137.299	106.377	0.0	0.9	0.0	0.0	0.0	0.0	0.0	0.0	0.0	0.0
5	70.7213	87.4649	106.585	0.0	0.9	0.0	0.0	0.0	0.0	0.0	0.0	0.0	0.0
6	57.6132	127.072	126.639	0.0	0.9	0.0	0.0	0.0	0.0	0.0	0.0	0.0	0.0
7	124.337	129.754	123.662	0.0	0.9	0.0	0.0	0.0	0.0	0.0	0.0	0.0	0.0
8	92.3978	39.2397	157.886	0.0	0.9	0.0	0.0	0.0	0.0	0.0	0.0	0.0	0.0
9	49.6695	122.844	109.999	0.0	0.9	0.0	0.0	0.0	0.0	0.0	0.0	0.0	0.0
10	85.0928	154.876	28.109	0.0	0.9	0.0	0.0	0.0	0.0	0.0	0.0	0.0	0.0
11	129.796	134.4	113.798	0.0	0.9	0.0	0.0	0.0	0.0	0.0	0.0	0.0	0.0
12	157.604	123.017	139.323	0.0	0.9	0.0	0.0	0.0	0.0	0.0	0.0	0.0	0.0
13	125.805	119.098	115.226	0.0	0.9	0.0	0.0	0.0	0.0	0.0	0.0	0.0	0.0
14	43.3195	94.929	121.213	0.0	0.9	0.0	0.0	0.0	0.0	0.0	0.0	0.0	0.0
15	133.874	68.524	92.6674	0.0	0.9	0.0	0.0	0.0	0.0	0.0	0.0	0.0	0.0
16	75.6714	58.4461	71.4934	0.0	0.9	0.0	0.0	0.0	0.0	0.0	0.0	0.0	0.0
17	46.5282	147.168	97.3119	0.0	0.9	0.0	0.0	0.0	0.0	0.0	0.0	0.0	0.0
18	152.497	137.709	125.681	0.0	0.9	0.0	0.0	0.0	0.0	0.0	0.0	0.0	0.0
19	98.3183	165.38	67.153	0.0	0.9	0.0	0.0	0.0	0.0	0.0	0.0	0.0	0.0
20	79.5993	149.82	52.2591	0.0	0.9	0.0	0.0	0.0	0.0	0.0	0.0	0.0	0.0
21	36.4946	60.9382	153.681	0.0	0.9	0.0	0.0	0.0	0.0	0.0	0.0	0.0	0.0
22	70.4785	82.109	48.8855	0.0	0.9	0.0	0.0	0.0	0.0	0.0	0.0	0.0	0.0
23	106.119	73.5643	78.9196	0.0	0.9	0.0	0.0	0.0	0.0	0.0	0.0	0.0	0.0
24	97.7808	163.754	10.5544	0.0	0.9	0.0	0.0	0.0	0.0	0.0	0.0	0.0	0.0
25	89.4892	25.9438	143.194	0.0	0.9	0.0	0.0	0.0	0.0	0.0	0.0	0.0	0.0
26	95.5874	145.507	12.3958	0.0	0.9	0.0	0.0	0.0	0.0	0.0	0.0	0.0	0.0
27	92.2248	44.0145	123.393	0.0	0.9	0.0	0.0	0.0	0.0	0.0	0.0	0.0	0.0
28	92.0574	28.2227	118.576	0.0	0.9	0.0	0.0	0.0	0.0	0.0	0.0	0.0	0.0
29	127.57	40.5684	149.863	0.0	0.9	0.0	0.0	0.0	0.0	0.0	0.0	0.0	0.0
30	88.0377	137.021	5.05667	0.0	0.9	0.0	0.0	0.0	0.0	0.0	0.0	0.0	0.0
31	132.299	59.7974	96.2598	0.0	0.9	0.0	0.0	0.0	0.0	0.0	0.0	0.0	0.0
32	67.5908	133.668	91.4681	0.0	0.9	0.0	0.0	0.0	0.0	0.0	0.0	0.0	0.0
33	99.4108	159.175	69.8968	0.0	0.9	0.0	0.0	0.0	0.0	0.0	0.0	0.0	0.0
34	29.8024	142.437	127.803	0.0	0.9	0.0	0.0	0.0	0.0	0.0	0.0	0.0	0.0
35	161.537	149.206	155.136	0.0	0.9	0.0	0.0	0.0	0.0	0.0	0.0	0.0	0.0
36	114.542	85.0376	72.2146	0.0	0.9	0.0	0.0	0.0	0.0	0.0	0.0	0.0	0.0
37	124.81	135.859	117.022	0.0	0.9	0.0	0.0	0.0	0.0	0.0	0.0	0.0	0.0
38	131.537	116.449	114.799	0.0	0.9	0.0	0.0	0.0	0.0	0.0	0.0	0.0	0.0

Fig. 17. Analysis conducted on the same CBCT shows zero changes proving that, if we exclude the error from segmentation and registration, the program has a perfect sensitivity.

Since the methodology used in this study is novel, an accurate pipeline validation is required. Some data to prove the validity of this system have been obtained using the same CBCT for one patient (Fig.17) and two different CBCTs taken on the same patient before and after treatment (Fig. 18). Using the same CBCT showed a perfect value of sensitivity, eliminating the errors that can be generated from segmentation and

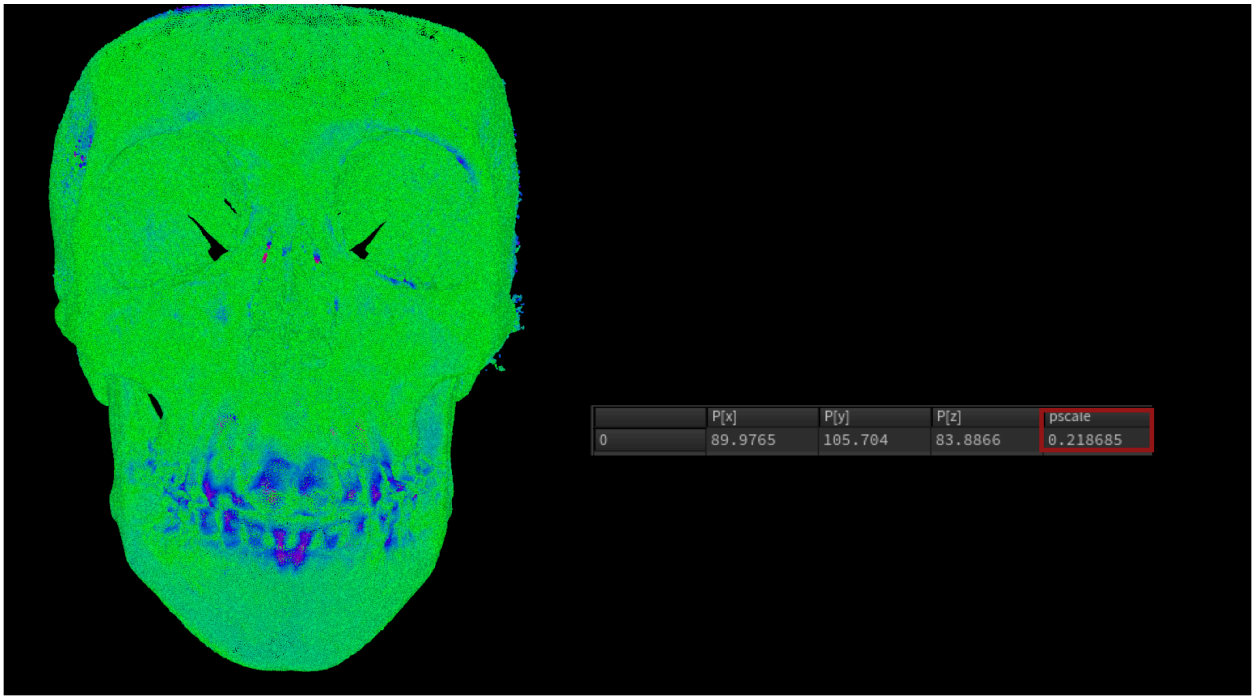

Fig. 18. Analysis conducted on a patient treated with Motion appliance: no significant skeletal changes in the upper and middle face are shown except some noise in areas that the automated segmentation tends to produce some distortion. The most significant changes are detected on the dentition level as a consequence of orthodontic treatment.

registration of the CBCT. The method proved to be absolutely valid showing no variation or movement at all for all of the 1 million points (Fig.). When using the CBCT taken on a patient treated with Motion Distalizer (Henry Schein Dental, Melville, New York, U.S.), no significant changes had been shown on the upper and middle face except in some of the areas where the segmentation always carried some noise. The effect on the dentition is

otherwise clear, with the lower incisors having the highest movement due to the use of Class II elastics and resolution of the anterior lower crowding that the patient presented at the beginning of treatment showing a good specificity. We determined the P-scale as the average of the movements that the 1,000,000 points underwent. Thus, including the points located on the dentition, the average displacement was 0.22 mm. However, this cannot be considered the mean error because it has been done on one patient due to the difficulty of finding controls. To calculate the actual error, the displacement in the dentition area should be subtracted from the overall average displacement since such displacement at the dentition level is expected due to the patient's orthodontic treatment.

The ideal control to validate the workflow would be to obtain two CBCTs from the same patient taken at two different timepoints without any orthodontic intervention. However, this proves difficult for ethical reasons and such data did not exist in our database.

The absence of a real point-to-point correspondence represents another limitation of this study. Currently, there is no automated algorithm developed to create a Non-Rigid Iterative Point-to-Point correspondence. In response, the lab team attempted to utilize cephalometric landmarks on the pre- and post-segmented skull surfaces to guide the creation of a true point-to-point correspondence. However, the points used as reference underwent severe displacement and were difficult to trace accurately between the pre- and post- expansion skulls, also suggesting a high level of operator error in point plotting. Ultimately, a modified closest point correspondence algorithm was used as an alternative, as previously explained, to maximize the accuracy of the results. It must not be

discounted, however, that the use of several steps in this analysis might introduce more processing errors.

While the amount of information carried by the program is highly valuable for research purposes, it may be difficult to implement it into the clinical setting. This information overload must be streamlined for the average orthodontist to be of greater practical use.

FUTURE DIRECTIONS

The field of medicine is seeing increasing innovation in 3D analysis methodology and investment into surface mapping and quantification of 3D data. In relation to this study, the goal is to establish a more accurate point-to-point correspondence method. Trends in technology are moving toward automation by machine-learn processing and/or artificial intelligence (AI), where software systems are able to automatically detect true point-to-point correspondence. Until then, a smaller step toward automation could be to utilize a smaller number of points that are more stable and easier to identify to guide the software into an even more accurate point-to-point correspondence.

In order to bridge the gap between clinical and translational research, a more user-friendly interface can be created for orthodontists to better monitor the changes in their patients as a result of their treatment. Currently there are various softwares in the market that provide solely visual tools to track these changes, but 3D quantification of such data is greatly lacking. Introduction of this 3D tool would be of great interest for every practitioner seeking to quantify and compare the effect of their intervention using different orthodontic mechanics and appliances. Making this tool more user-friendly would entail, for instance, the development a simplified vector map, which would reduce the 1 million vectors by averaging their displacement and direction according to specific areas of interest.

As discussed previously in the limitations, the ideal control would be represented by a series of two consecutive CBCTs from the same subject without any surgical or

orthodontic intervention. It is a clear ethical dilemma to unnecessarily expose subjects to double radiation. As an alternative, non-growing patients that underwent orthodontic treatment could be used as controls. In this scenario, only dental changes should be detected with little to no skeletal changes. However, the UCLA Orthodontics database does not have sufficient pre- and post-CBCTs of patients treated with conventional orthodontic mechanics.

The patients used in this investigation have also been the subjects for airway analysis research, from which inspiratory flow measurements[23] and airway volume changes have been studied. It would be of great clinical and research interest to consolidate and compare our team findings and correlate the data. In doing so, we can assess the relationship between the amount of skeletal expansion, increase in airway volume and respiratory flow improvement.

The same program could be used in 3D cephalometric analysis, which has been the focus of orthodontic research in the past decade. This can be achieved by creating different population norms in the form of an average skull and use it to establish the variation of our patients by direct comparison of the individual skull to the established norm.

The data could potentially be divided into subcategories such as the amount of expansion, the age or sex of the patient and compared with the skeletal effects achieved, helping to improve our clinical understanding of the effect of MSE.

A direct continuation of this research project involves the implementation of a third time point for post-orthodontic treatment (T2) to evaluate stability of skeletal expansion.

Some preliminary data demonstrating some minor skeletal relapse in the final timepoint compared to the immediate post expansion results are shown in Fig. 19.

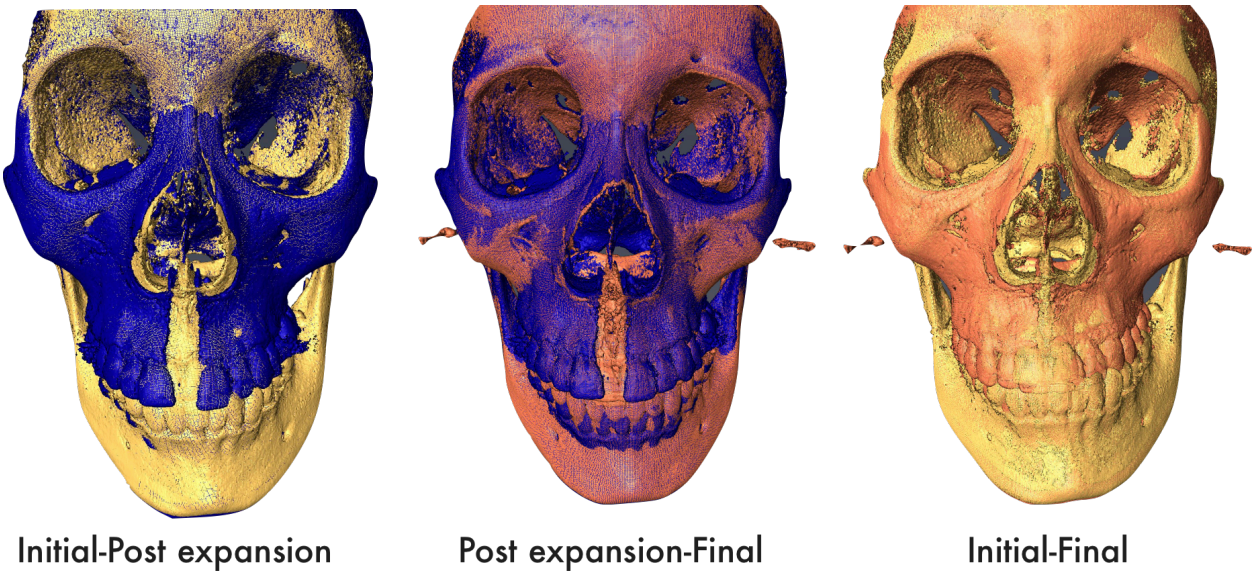

Fig. 19. Preliminary data showing the registration and segmentation of one sample including the final/post treatment timepoint.

REFERENCES

1. Brunelle JA., Bhat M., et al., Prevalence and distribution of selected occlusal characteristics in the US population, 1988-1991. J Dent Res. 1996 Feb; 75 Spec No:706-13.

2. Kutin G, Hawes RR. Posterior cross-bites in the deciduous and mixed dentitions. Am J Orthod. 1969; 56(5):491–504.

3. Egermark-Eriksson I, Carlsson GE, Magnusson T, Thilander B. A longitudinal study on malocclusion in relation to signs and symptoms of cranio-mandibular disorders in children and adolescents. Eur J Orthod. 1990; 12(4):399–407.

4. Kutin G., Hawes RR., Posterior cross-bites in the deciduous and mixed dentitions. American Journal of Orthodontics and Dentofacial Orthopedics. 1969 Nov; 56(5):491- 504.

5. Mossey P. The heritability of malocclusion: part 2. The influence of genetics in malocclusion. Br J Orthod 1999; 26:195–203

6. Gungor A., Turkkahramanb G. Effects of Airway Problems on Maxillary Growth: A Review. European Journal of Dentistry. 2009; 3:250-254

7. Ashok N., Varma NK, Ajith VV, Ramesh N. Dentofacial Effects of Rapid Maxillary Expansion Amrita Journal of Medicine Vol. 10, No: 2 July - Dec 2014. Page 1 – 44

8. Bishara SE, Staley RN. Maxillary expansion: clinical implications. Am J Orthod Dentofacial Orthop 1987;91:3-14.

9. Garib DG, Henriques JF, Janson G, Freitas MR, Coelho RA. Rapid maxillary expansion--tooth tissue-borne versus tooth-borne expanders: a computed tomography evaluation of dentoskeletal effects. Angle Orthod. 2005 Jul;75(4):548-57

10. Farhan Bazargani; Ingalill Feldmann; Lars Bondemark Three-dimensional analysis of effects of rapid maxillary expansion on facial sutures and bones. A systematic review. Angle Orthod. 2013 Nov;83(6):1074-82.

11. Linder-Aronson, S., & Lindgren, J. (1979). The Skeletal and Dental Effects of Rapid Maxillary Expansion. British Journal of Orthodontics, 6(1), 25–29.

12. Haofu Lee, Kang Ting, Michael Nelson, Nichole Sun, and Sang-Jin Sung. Maxillary expansion in customized finite element method models. Am J Orthod Dentofacial Orthop. 2009 Sep;136(3):367-74

13. Weissheimer A, de Menezes LM, Mezomo M, Dias DM, de Lima EM, Rizzatto SM. Immediate effects of rapid maxillary expansion with Haas-type and hyrax-type expanders: a randomized clinical trial. Am J Orthod Dentofacial Orthop. 2011;140:366-376.

14. Stuart Da, Wiltshire WA. Rapid Palatal Expansion in the Young Adult: Time for a Paradigm Shift? J Can Dent Assoc. 2003 Jun;69(6):374-7.

15. Kumar SA, Gurunathan D., Muruganandham, Sharma S. Rapid Maxillary Expansion: A Unique Treatment Modality in Dentistry. Journal of Clinical and Diagnostic Research. 2011 August, Vol-5(4): 906-911.

16. Hyun-Mook Lim, Young-Chel Park, Kee-Joon Lee, Kyung-Ho Kim, and Yoon Jeong Choi. Stability of dental, alveolar, and skeletal changes after miniscrew-assisted rapid palatal expansion. Korean J Orthod. 2017 Sep; 47(5): 313–322.

17. Suri L, et al. Surgically Assisted Rapid Palatal Expansion: A Literature Review. Am J Orthod Dentofacial Orthop. 2008; 133(2): 290-302. 1.

18. Suresh Menon, Ravi Manerikar, Ramen Sinha. Surgical Management of Transverse Maxillary Deficiency in Adults. J Maxillofac Oral Surg. 2010 Sep;9(3):241-6

19. Lu Lin; Hyo-Won Ahn; Su-Jung Kim; Sung-Chul Moon; Seong-Hun Kim; Gerald Nelson Tooth-borne vs bone-borne rapid maxillary expanders in late adolescence. Angle Orthod. 2015 Mar;85(2):253-62

20. Carlson C, Sung J, McComb RW, Machado AW, Moon W. Microimplant-assisted rapid palatal expansion appliance to orthopedically correct transverse maxillary deficiency in an adult. Am J Orthod Dentofacial Orthop. 2016 May; 149(5): 716-728

21. Daniel Paludo Brunetto, Eduardo Franzzotti Sant'Anna, Andre Wilson Machado, Won Moon. Non-surgical treatment of transverse deficiency in adults using Microimplant-assisted Rapid Palatal Expansion (MARPE). Dental Press J Orthod. 2017 Jan-Feb;22(1):110-25

22. Lee RJ, Moon W, Hong C. Effects of monocortical and bicortical mini-implant anchorage on bone-borne palatal expansion using finite element analysis. Am J Orthod Dentofacial Orthop. 2017;151(5):887–897.

23. Storto CJ, Garcez AS, Suzuki H, Cusmanich KG, Elkenawy I, Moon W, Suzuki SS. Assessment of respiratory muscle strength and airflow before and after microimplant-assisted rapid palatal expansion. Angle Orthod. 2019 Mar 21.

24. Daniele Cantarella, Ramon Dominguez-Mompell, Christoph Moschik, Sanjay M. Mallya, Hsin Chuan Pan, Mohammed R. Alkahtani,aIslam Elkenawy, and Won Moon. Midfacial changes in the coronal plane induced by microimplant-supporter skeletal expander, studied with cone-beam computed tomography images. Am J Orthod Dentofacial Orthop 2018;154:337-45

25. Daniele Cantarella,et al. Changes in the midpalatal and pterygopalatine sutures induced by microimplant- supported skeletal expander, analyzed with a novel 3D method based on CBCT imaging. Progress in Orthodontics (2017)

26. Daniele Cantarella et al. Zygomaticomaxillary modifications in the horizontal plane induced by micro-implant supported skeletal expander, analyzed with CBCT images Progress in Orthodontics (2018).

27. Lin Y. Comparison of skeletal and dental changes with MSE (Maxillary Skeletal Expander) and Hyrax appliance using CBCT imaging. A thesis submitted in partial satisfaction of the requirements for the degree of Master of Science in Oral Biology

28. Sara Abedini et al. Three-dimensional soft tissue analysis of the face following micro-implant-supported maxillary skeletal expansion. Progress in Orthodontics (2018)

29. MacGinnis et al. The effects of micro-implant assisted rapid palatal expansion (MARPE) on the nasomaxillary complex —a finite element method (FEM) analysis. Progress in Orthodontics. 2014 15:52.

30. Moon W, Wu KW, MacGinnis M, Sung J, Chu H, Youssef G and Machado A. The efficacy of maxillary protraction protocols with the micro-implant-assisted rapid palatal expander (MARPE) and the novel N2 mini-implant—a finite element study. Progress in Orthodontics (2015) 16:16

31. Cevidanes LH, Styner MA, Proffit WR.Image analysis and superimposition of 3-dimensional cone-beam computed tomography models. Am J Orthod Dentofacial Orthop 2006;129:611-8.

32. Cevidanes LH, Bailey LJ, Tucker GR Jr, Styner MA Superimposition of 3D cone-beam CT models of orthognathic surgery patients. Dentomaxillofac Radiol. 2005 Nov;34(6):369-75

33. Cevidanes LH, Heymann G, Cornelis MA, DeClerck HJ. Superimposition of 3-dimensional cone-beam computed tomography models of growing patients. Am J Orthod Dentofacial Orthop. 2009 July ; 136(1): 94–99

34. Frederik Maes F., Vandermeulen D., and Paul Suetens. Medical Image Registration Using Mutual Information. Proceedings of the ieee, vol. 91, no. 10, october 2003

35. Weissheimer A, Menezes LM, Koerich L, Pham J, Cevidanes LH. Fast three-dimensional superimposition of cone beam computed tomography for orthopaedics and orthognathic surgery evaluation. Int J Oral Maxillofac Surg. 2015;44(9):1188-1196

36. Ghoneima,H. Cho,K. Farouk, K. Kula. Accuracy and reliability of landmark-based, surface-based and voxel-based 3D cone-beam computed tomography superimposition methods. No statistical significance showed. Orthod Craniofac Res. 2017 Nov;20(4):227-236

37. Yushkevich PA, Piven J, Hazlett HC, Smith RG, Ho S, Gee JC, et al. User-guided 3D active contour segmentation of anatomical structures: Significantly improved efficiency and reliability. NeuroImage. 2006 Jul;31(3):1116–28.

38. Schilling J, Gomes LCR, Benavides E, et al. Regional 3D superimposition to assess temporomandibular joint condylar morphology. Dentomaxillofacial Radiology. 2014;43(1):20130273.

39. Josef Freudenthaler et al. Geometric morphometrics of different malocclusions in lateral skull radiographs. J Orofac Orthop. 2017

40. Bookstein FL et al. Landmark methods for forms without landmarks: morphometrics of group differences in outline shape. Med Image Anal. 1997

41. Mitteroecker PM et al. Advances in geometric morphometrics. Evol Biol. 2009

42. Halazonetis DJ et al. Morphometrics for cephalometric diagnosis. Am J Orthod Dentofacial Orthop. 2004

43. John M. Starbuck et al. Bilateral cleft lip and palate: A morphometric analysis of facial skeletal form using cone beam computed tomography. Clin. Anat 2015

44. Belden CJ. The skull base and calvaria. Adult and pediatric.Neuroimaging Clin N Am 1998;8:1-20.

45. R.J. Hennessy et al. Facial growth: separating shape from size. Eur J Orthod, 23 (2001), pp. 275–285

46. G.D. Singh et al. Craniofacial heterogeneity of prepubertal Korean and European-American subjects with Class III malocclusions: Procrustes, EDMA, and cephalometric analyses. Int J Adult Orthod Orthognath Surg, 13 (1998), pp. 227–240

47. L. Franchi et al. Thin-plate spline analysis of the short- and long-term effects of rapid maxillary expansion. Eur J Orthod, 24 (2002), pp. 143–150